FC

DESIGN PARAMETERS FOR SUBSONIC AIR-AIR EJECTORS

BY

J. W. MITCHELL

TECHNICAL REPORT NO. 40

PREPARED UNDER CONTRACT Nonr 225(23)
(NR-090-342)
FOR
OFFICE OF NAVAL RESEARCH

DEPARTMENT OF MECHANICAL ENGINEERING
STANFORD UNIVERSITY
STANFORD, CALIFORNIA

DECEMBER 31, 1958

DESIGN PARAMETERS FOR SUBSONIC AIR-AIR EJECTORS

Technical Report No. 40

Prepared under Contract Nonr 225(23)
(NR-090-342)

For
Office of Naval Research

Department of Mechanical Engineering
Stanford University
Stanford, California

December 31, 1958

Report Prepared By:

J. W. Mitchell

Approved By:

A. L. London

Project Supervisor

ABSTRACT

The present extensive use of the ejector as a fluid pump has brought into focus the need for an adequate ejector design procedure. An analysis is presented that provides a relation for ejector behavior in terms of the governing non-dimensional parameters. Model tests are presented which a) verify the analysis, and b) establish the numerical values for the two design coefficients that are required.

The intended application of this procedure was originally one involving the exhaust of a gas turbine as the driving fluid. The numerical values of the parameters have been confined to a range consistent with this application, and in this sense only the analysis is limited.

This study is a direct extension of the program previously reported in references (1) and (2).

ACKNOWLEDGEMENT

The advice and suggestions of Professor A. L. London are most sincerely appreciated.

TABLE OF CONTENTS

LIST OF FIGURES

LIST OF FIGURES (Cont'd)

LIST OF TABLES

REFERENCES

1. "Exhaust-Stack Ejectors for Marine Gas Turbine Installations," by A. L. London and P. F. Pucci, TR-No. 26, Contract N6onr 251 Task 6, Department of Mechanical Engineering, Stanford University, 1955.

2. "Simple Ejector Design Parameters," by P. F. Pucci, PhD Thesis, Department of Mechanical Engineering, Stanford University, 1954.

3. "Gas Tables," by J. H. Keenan and J. Kaye, John Wiley and Sons, 1949.

4. "Investigation of Flow in an Axially Symmetrical Heated Jet of Air," by S. Corrisin, NACA ACR 3L23.

5. "Aerodynamics of Propulsion," by D. Kuchemann and J. Weber, McGraw-Hill Book Co., 1953.

6. "A Note on the Measurement of Total Head and Static Pressure in a Turbulent Stream," by S. Goldstein, Proc. Royal Society, Series A, Vol. 155, No. 188, pp. 570-575.

7. "Effect of Turbulence on Air Flow Measurements Behind Orifice Plates," by J. N. Nielson, NACA WR L-274.

8. "Aerodynamic Measurements," by R. C. Dean, M.I.T. Gas Turbine Laboratory, 1953.

9. "The Turbulent Mixing of Co-Axial Gas Jets," by F. Landis and A. H. Shapiro, Heat Transfer and Fluid Mechanics Institute, 1951, pp. 133-147.

10. "Momentum and Mass Transfer in Co-Axial Gas Jets," by W. Forstall and A. H. Shapiro, Jour. of Applied Mechanics, December 1950, p. 399.

NOMENCLATURE

English Letter Symbols

A	area, ft^2. A_1, A_2, A_o, A_s, and A_m are flow areas defined in the ejector sketches, Figs. 1 and 2. A_w is the mixing tube wall area.
C_1, C_2, C_3	coefficients defined by equation set [13a]
D	diameter of the mixing tube, ft
f	flow friction factor, dimensionless
F_{fr}	wall friction shear force, #
g_c	32.20 ft lb/# sec^2, the reciprocal of the proportionality factor in Newton's Second Law; force, length, mass, and time are the primary quantities.
h	enthalpy, ft #/lb or Btu/lb . h_m, h_p, h_s apply to the mixed, primary, and secondary flow streams respectively.
L	length of the mixing tube, ft
M	molal mass of gas, 29.0 lbs/lb mol for air
P	gas pressure, #/ft^2
ΔP	pressure difference, #/ft^2 or inches of water
R	the universal gas constant, 1545 ft #/(lb mol R)
T	absolute temperature, R
U	local velocity at a point in the flow cross section, ft/sec
V	bulk average velocity at a flow cross section, ft/sec. V_m, V_p, V_s apply to the mixed, primary, and secondary flow streams respectively at the sections indicated in Fig. 1.
v	gas specific volume ($1/\rho$), ft^3/lb
w	flow rate, lbs/sec. w_m, w_p, w_s apply to the mixed, primary, and secondary flow streams respectively; see Figs. 1 and 2.
x	flow length position along the mixing tube measured from the throat of the secondary nozzle, ft

Greek Letter Symbols

Δ	on P denotes a pressure differential
$\emptyset$	denotes a functional relation
η	energy efficiency, dimensionless
ρ	gas density, lbs/ft^3
μ	gas viscosity, lbs/sec ft

Nondimensional Parameters for Ejector Performance

A*	the area parameter, secondary to primary flow area ratio
K_m	momentum correction factor relating the actual flow stream momentum rate to that calculated from the bulk average velocity, see Eq. [5]
K_p	static pressure correction factor relating the actual pressure in the exit plane to the static pressure at the ejector wall at the exit, see Eq. [4]
K_p^*	exit static pressure variation coefficient
L/D	length parameter for the ejector
ΔP^*	pressure coefficient, a measure of ejector performance when correlated with W*
T*	the temperature parameter, secondary to primary stream temperature ratio
W*	the flow rate parameter, secondary to primary stream flow rate ratio, a measure of ejector performance when correlated with ΔP^*

Miscellaneous

#	denotes pounds <u>force</u> in distinction to
lbs	denoting pounds <u>mass</u>

INTRODUCTION

The current status of ejector design information represents, primarily, the fruits of a "cut-and-try" approach to the problem of ejector development. The lack of a systematic and rational design method instigated the present investigation, of which the preliminary results were reported in (1) and (2)*. This investigation has been focused on a specific application -- the use of the exhaust of a gas turbine as the driving medium to pump a supply of ventilating air for the machinery space. This application is characterized by:

a. A medium subsonic velocity, high temperature, driving fluid (exhaust gases) of essentially the same molecular weight as the pumped secondary fluid (air).
b. A secondary stream of ventilating air at low temperatures (80 to 120°F).
c. A ratio of secondary to primary flow areas in the range 1 to 10.
d. A circular mixing duct of constant cross sectional area in which the momentum transfer between the primary and secondary fluids occurs.

These are the characteristics of prime mover installations in test cells, vehicles, and ships incorporating ejector-driven ventilating and cooling systems.

The preliminary results of the model tests of an ejector with these characteristics were reported in (1) and (2). This initial study established the following:

1. An analytical relation for the prediction of ejector performance. The incoming primary and secondary velocity and temperature distributions are assumed uniform over the primary and secondary areas, respectively. The nonuniform velocity and temperature profiles at the exit of the ejector mixing

---

*Numbers in parentheses refer to the References.

tube are accounted for by a nondimensional momentum correction factor, K_m, modifying the momentum rate based on the bulk average mass velocity.

2. The relations between the K_m factor and the design variables -- area ratio, flow rate ratio, temperature ratio, and duct length to diameter ratio. These relations, established by model tests, are required for the solution of the ejector design problem.

3. An analysis tentatively indicating that the number of governing nondimensional parameters could be reduced. The secondary to primary temperature ratio, T^*, was combined with secondary to primary flow rate ratio, W^*, in the form $W^*T^{*0.5}$ to provide a correlation for the K_m factor. It was also seen that if these two parameters were combined as $W^*T^{*0.4}$, the nondimensional ejector performance parameter, $\Delta P^*/T^*$ was successfully correlated. In this way T^* was eliminated as a separate parameter; as this conclusion was based on analysis, experimental confirmation is needed.

The present study is an extension of the foregoing work, reported in (1) and (2), with the following objectives:

1. Experimental justification for $W^*T^{*0.5}$ as a correlating parameter for the momentum correction factor K_m.
2. Experimental justification for $W^*T^{*0.4}$ as a correlating parameter for ejector performance $\Delta P^*/T^*$.
3. A refinement of the previous modified one-dimensional analysis with the introduction of a static pressure correction factor K_p to account for the nonuniform static pressure at the ejector exit.
4. Development of a less tedious and more accurate method of determining the momentum correction factor K_m instead of the previously used Pitot tube and temperature probe traversing procedures followed by an integration of the momentum flux over the cross section.
5. A revision and extension of the design curves presented in (1) as a result of the investigations under

3 and 4.

6. Some performance results for a combination of constant area and constant pressure mixing.

SUMMARY AND CONCLUSIONS

The analysis and discussion of the model test results, which are presented in the later sections of this work, lead to the following conclusions:

1. It is empirically demonstrated that the momentum correction factor K_m (defined by Eq. [5]) is effectively correlated by combining the flow rate and temperature parameters, W^* and T^*, in the form $W^*T^{*0.5}$ (Figs. 6 and 7). The correlation of K_m with $W^*T^{*0.5}$, as opposed to W^* alone, reduces the spread of the data by factors of 2 to 1 to 10 to 1. This further reinforces the hypothesis regarding $W^*T^{*0.5}$ as a correlating factor (1).

2. It is empirically demonstrated that $W^*T^{*0.4}$ effectively correlates $\Delta P^*/T^*$ (Figs. 4 and 5); this verifies the conclusion reached analytically that W^* and T^* can be combined as $W^*T^{*0.4}$ for all $T^* \geq 0.3$, (1). The difference between the K_m correlating factor ($W^*T^{*0.5}$) and the $\Delta P^*/T^*$ correlating factor ($W^*T^{*0.4}$) is discussed in the text.

3. A static correction factor, K_p, which accounts for the nonuniformity of static pressure at the jet exit, is introduced into the one-dimensional design equation. K_p is defined by Eq. [4]. The departure of K_p from unity is a measure of its influence on performance. For $L/D < 6$ and $A^* > 5$ (Fig. 12), the effect on ΔP^* can amount to 20 per cent. The use of both K_m and K_p in the design equation allows an accurate prediction of ejector performance. (In Figs. 4 and 5, the influence is minor.)

4. A more accurate method of determining K_m by experiment for low L/D's is to compute it from the performance results using the design equation [13]. This procedure differs from the previous one, (2), of evaluating K_m from velocity and temperature traverses of the mixing tube flow. The uncertainty in K_m is reduced substantially for L/D's less than 4. For larger L/D's, the traverse method yields accurate results. The overall performance method is used in the evaluation of K_m for Figs. 13, 14, and 15.

5. On the basis of the present model test results, the K_m design curves of (1) are revised and extended for L/D's of 1, 2, and 3 (Figs. 13, 14, 15). For L/D's greater than 4, no revision was necessary; here Fig. 16 is Fig. 21 of (1). The revision for L/D's of 1, 2, and 3 was necessary due to a change in flow pattern as discussed in the text. The K_m results are presented as a function of A^*, with $W^*T^{*0.5}$ as a parameter. The range of A^*'s tested extends from 1 to 7, the range of L/D's 1 to 8. This range of A^*'s and L/D's will include most ejector design applications for which the primary (driving) stream is of necessity a low or medium subsonic speed flow (e.g. exhaust from a gas turbine, diesel, or similar prime mover).

6. The maximum $W^*T^{*0.4}$ possible in an ejector is presented as a function of A^*, with L/D as a parameter (Fig. 17). This characteristic is determined from the design equation [13] with $\Delta P^*/T^* = 0$. These characteristics define the limits of ejector flow rate performance and aid in specifying the conditions for W^* and ΔP^* for maximum efficiency (see Application to Design).

7. Some limited results are presented for ejector performance with the primary nozzle discharge displaced from the throat of the secondary nozzle (Fig. 18). For the A^* tested (1.835), gains of 3% to 10% in $W^*T^{*0.4}$ were realized. The maximum gains occurred at the highest $W^*T^{*0.4}$'s. The primary nozzle discharge was displaced about one mixing tube diameter from the throat of the secondary nozzle into the plenum chamber to obtain this maximum. The optimum distance into the plenum chamber decreased as $W^*T^{*0.4}$ was decreased. The variation of $W^*T^{*0.4}$ with primary nozzle displacement revealed that the ejector performance is relatively insensitive to small displacements of the primary nozzle from the throat of the secondary nozzle (Fig. 19).

8. An ejector design procedure illustrating the use of the design curves is presented in the APPLICATION TO DESIGN section, page 29.

9. It is believed that the simple ejector problem has been satisfactorily solved in its more essential features, at least from the designers' viewpoint. The evident research problems remaining are:

a. Determination of the optimum primary nozzle location.

b. Effect of secondary nozzle shape on ejector performance together with primary nozzle location.

c. Analytical study of the mixing process, with the prediction of velocity, temperature, and pressure distributions as a goal so as to supplant the present empirical procedure of establishing K_m and K_p.

ANALYSIS

A simple analysis follows, closely paralleling that presented in (1),for the ejector system described by Fig. 1. The ejector primary stream discharge is the throat location configuration of Fig. 2a; the primary nozzle discharge coincides with the throat of the secondary nozzle. The following analysis is presented specifically for this geometry.

The primary flow, w_p , enters the mixing tube at section 1 through a nozzle of area A_p with a velocity V_p . This primary flow induces a secondary flow, w_s , which enters section 1 through an annulus of area A_s with a velocity V_s . The resulting mixed flow, $w_m = w_p + w_s$, leaves the mixing tube at section 2 with mean velocity V_m . The primary velocity, V_p , is greater than the secondary velocity, V_s . The corresponding temperatures and densities are also shown in Fig. 1.

The equations for ejector performance are established by combining the equations of continuity, energy, momentum, and state, the Second Law of Thermodynamics, the defining equations for K_m and K_p , and the prescribed boundary conditions. In addition the following idealizations and definitions are employed:

1. Steady-state flow between sections 0 to 1 and 1 to 2 (Fig. 1).

2. Adiabatic flow throughout with one-dimensional isentropic flow (reversible adiabatic) of the secondary stream from section 0 to 1, and irreversible adiabatic mixing of the primary and secondary flow streams between section 1 and 2.

3. At section 1, the stream velocities, V_p and V_s , and temperatures, T_p and T_s , are uniform across their respective streams. However, V_p is not equal to V_s and T_p is not equal to T_s , (Fig. 1).

4. Nonuniform accelerations and deaccelerations result in a nonuniform static pressure distribution across the stream at sections 1 and 2. This static pressure distribution is

accounted for by a nondimensional pressure correction factor, K_p, relating the actual static pressure across the mixing tube to the wall pressure at that section. It was experimentally determined that the wall pressure at exit is equal to atmospheric pressure; hence $K_p P_2 = P_a$. The specification of one-dimensional isentropic flow from section 0 to 1 makes $K_p \equiv 1$ at section 1 since the static pressure is uniform in the plenum chamber (section 0).

5. Incomplete mixing of the primary and secondary streams between sections 1 and 2 and wall friction result in a nonuniform velocity distribution which may be accounted for by the use of a momentum correction factor, K_m, (nondimensional) which relates the actual momentum rate at section 2 to the nominal rate based on the bulk average velocity and density at section 2.

6. Both flows behave as perfect gases and, moreover, their molal masses (molecular weights) and other thermal properties approximate those of air at the appropriate temperatures.

7. Wall friction between sections 1 and 2 is accounted for with a conventional friction-factor term based on the bulk flow velocity V_m and the mixing tube wall area A_w (Eq. [6]).

8. Pressure changes, P_0 to P_1, and P_i to P_2, are small relative to the static pressure so that the gas density is essentially dependent on temperature (and atmospheric pressure).

9. Flow potential energy of position and kinetic energy changes are relatively negligible for the purpose of evaluating the bulk average temperature at section 2.

The Continuity Equation -- The conservation of mass principle, applied to the mixing tube between sections 1 and 2 as a control volume, yields:

$$w_m = w_p + w_s \qquad [1]$$

where

$$w_m = (\rho_m A_m V_m)_2 \quad ; \quad w_p = (\rho_p A_p V_p)_1 \; ; \; w_s = (\rho_s A_s V_s)_1 \qquad [1a]$$

The Energy Equation -- The conservation of energy principle, applied to the mixing tube between sections 1 and 2 as a control volume, yields:

$$w_m h_m = w_p h_p + w_s h_s \qquad [2]$$

where the potential energies of position and the kinetic energy terms are neglected (idealization 9), and the flow is adiabatic (idealization 2).

From the specification of perfect gas behavior (idealization 6):

$$T_m = \emptyset(h_m) \quad \text{only} \; ,$$

from equation of state considerations. Therefore, with the primary and secondary flow rates and temperatures known, and with the use of available equation of state data (3), T_m can be calculated.

The Momentum Equation -- The conservation of momentum principle, applied to the mixing tube between sections 1 and 2 as a control volume, yields:

$$\frac{w_p V_p}{g_c} + \frac{w_s V_s}{g_c} + P_1 A_1 = K_m \frac{w_m V_m}{g_c} + (K_p P_2) A_2 + F_{fr} \qquad [3]$$

From the specified geometry, $A_1 = A_2$ (Fig. 1). Idealization 3 allows the use of $(w_p V_p)/g_c$ and $(w_s V_s)/g_c$ as the primary and secondary momentum rates at section 1, respectively. Specifications 4 and 5 allow the introduction of K_p and K_m to express the pressure force and momentum rate at section 2.

The Static Pressure Correction Factor -- K_p , in Eq. [3], is defined by:

$$K_p \triangleq \frac{1}{P_{wall}} \int_{A_m} P \, d\left(\frac{A}{A_m}\right) \qquad [4]$$

where $P_{wall} = P_{atm}$ when $L/D = x/D$.

The Momentum Correction Factor -- K_m , in Eq. [3], is defined by:

$$K_m \triangleq \frac{1}{\rho_m V_m^2} \int_{A_m} \rho U^2 d\left(\frac{A}{A_m}\right) \qquad [5]$$

where V_m is the bulk average velocity defined by:

$$V_m \triangleq \frac{w_m}{\rho_m A_m} \qquad [1b]$$

The Perfect Gas Equation of State is used to evaluate ρ_m :

$$\rho_m = \frac{(K_p P_2)}{(R/M) T_m} \qquad [2a]$$

where T_m is the bulk mean temperature evaluated from Eq. [2]. $K_p P_2$ is the wall pressure measured at Section 2, modified by K_p to yield the average discharge pressure.

The wall skin-friction force F_{fr} is related to the bulk properties using idealization 7:

$$F_{fr} = f \cdot A_{wall} \left[\frac{V_m^2 \rho_m}{2g_c}\right]_2 \qquad [6]$$

A reasonable value of f is 0.003 , an average of a pipe-flow type friction factor and a flat-plate type friction factor. The value of f is not critical; a variation in f of three to one does not affect the prediction of ejector performance significantly (1).

The ejector "pumped head" performance is defined in terms of the plenum chamber pressure, P_o , and the discharge pressure $K_p P_2 = P_a$. With the assumption of isentropic secondary flow from section 0 to section 1 (idealization 2), the energy equation in differential form for the secondary flow process 0 to 1 is:

$$dh = -d\left(\frac{V^2}{2g_c}\right)$$

The kinetic energy at section 0 (the plenum chamber) is negligible. As the flow is isentropic, from the Second Law

considerations:

$$T\,ds = dh - v\,dP = 0$$

and for small pressure differences

$$v \triangleq 1/\rho \approx 1/\rho_s$$

a constant. Combining these relations and integrating from section 0 to 1 yields:

$$\frac{P_o - P_1}{\rho_s} = \frac{V_s^2}{2g_c} \qquad [7]$$

The Solution for Ejector Performance -- The solution for ejector performance is found by combining the preceding equations to yield:

$$(P_a - P_o) = \frac{1}{g_c A_m}\left\{\frac{w_p^2}{A_p\rho_p} + \frac{w_s^2}{A_s\rho_s}\left[1 - \frac{1}{2}\frac{A_m}{A_s}\right] - \frac{w_m^2}{A_m\rho_m}\left[K_m + \frac{f}{2}\frac{A_w}{A_m}\right]\right\} + P_a(1 - K_p) \qquad [8]$$

where A_p and ρ_p apply to the primary flow at section 1; A_s and ρ_s, the secondary flow at section 1; and K_m, K_p, A_m, and ρ_m, the mixed flow at section 2. This equation can now be used in design calculations for ejector performance.

If a diffuser having an efficiency η_D is introduced at the end of the ejector, an improved plenum chamber vacuum can be obtained for a given secondary flow rate. For the ejector with a diffuser the foregoing analysis may be extended to yield a modification of Eq. [8]:

$$(P_a - P_o) = \frac{1}{g_c A_m}\left\{\frac{w_p^2}{A_p\rho_p} + \frac{w_s^2}{A_s\rho_s}\left[1 - \frac{1}{2}\frac{A_m}{A_s}\right] - \frac{w_m^2}{A_m\rho_m}\left[K_m + \frac{f}{2}\frac{A_w}{A_m} - \underbrace{\frac{\eta_D}{2}\left(1 - \frac{A_m^2}{A_D^2}\right)}_{\text{Diffuser Term}}\right]\right\} + P_a(1 - K_p) \qquad [9]$$

where the diffuser efficiency is defined by:

$$\eta_D = \frac{(P_a - P_2)_{actual}}{(P_a - P_2)_{isentropic\ flow}} \qquad [10]$$

For small pressure differences relative to the total pressure, as considered here, "pressure" and "energy" diffuser efficiencies are essentially equal:

$$(P_a - P_2)_{actual} = \eta_D \cdot \rho_m \frac{V_m^2}{2g_c} \left[1 - \frac{A_m^2}{A_D^2} \right]$$

Nondimensional Parameters -- Several advantages are realized if the ejector design equation is presented in nondimensional form. Design calculations are more readily accomplished if nondimensional parameters are used, and the number of independent variables is reduced. Most important is the fact that the nondimensional parameters are needed to provide the criteria of similarity between model and prototype in order to establish K_p and K_m from the model tests.

The nondimensional parameters useful for this analysis are:

$\Delta P^* \triangleq \left[\frac{P_a - P_o}{\rho_s}\right] \Big/ \left[\frac{V_p^2}{2g_c}\right]$ a pressure coefficient which compares the "pumped head", $(P_a - P_o)/\rho_s$, for the secondary flow to the "driving head", $V_p^2/2g_c$, of the primary flow.

$W^* \triangleq w_s/w_p$ a flow rate ratio, secondary-to-primary mass flow rate.

$T^* \triangleq T_s/T_p$ an absolute temperature ratio. $T^* \equiv \rho_p/\rho_s$, a flow density ratio, since the exhaust gas is presumed to have close to the same molal mass as the ventilating air, and pressure differences are small relative to atmospheric pressure.

A_p/A_m, A_m/A_D, $A^* \triangleq A_s/A_p$; all flow area ratios defined by outer duct inside dimensions, primary tube ID, primary tube wall thickness, and diffuser discharge area.

A_w/A_m = wall friction area to mixing tube flow cross section area ratio.

K_p, K_m, f, η_D = the pressure correction factor, the momentum correction factor, the wall friction factor, and the diffuser efficiency. These design parameters have been previously considered.

$$K_p^* \triangleq \left[\frac{P_a(1 - K_p)}{\rho_s}\right] \Big/ \left[\frac{V_p^2}{2g_c}\right]$$ a convenient nondimensional grouping for the effect of nonuniform static pressure across the mixing tube exit on ejector performance.

Introducing these nondimensional parameters into Eq. [9]:

$$\frac{\Delta P^*}{T^*} = 2\left(\frac{A_p}{A_m}\right)\left\{1 + \frac{W^{*2}T^*}{A^*}\left[1 - \frac{1}{2A^*(A_p/A_m)}\right] - (1+W^*)(1+W^*T^*)\left(\frac{A_p}{A_m}\right)\left[K_m + \frac{f}{2}\frac{A_w}{A_m} - \frac{\eta_D}{2}\left(1 - \frac{A_m^2}{A_D^2}\right)\right]\right\} + \frac{K_p^*}{T^*} \quad [11]$$

For a fixed ejector geometry, Eq. [11] reduces to the form:

$$\frac{\Delta P^*}{T^*} = C_1 - C_2 W^{*2} T^* - C_3 W^*(T^* + 1) + \frac{K_p^*}{T^*} \quad [12]$$

where the C coefficients involve only geometry, K_m, f, and η_D. These are defined in the equation set [13a]. From Eq. [11]:

$$\frac{\Delta P^*}{T^*} = \phi[W^*, T^*, A^*, A_p/A_m, A_w/A_m, A_D/A_m, K_m, K_p, f, \eta_D]$$

With the geometry established, $\Delta P^*/T^*$ becomes a function of only five parameters (W^*, T^*, K_m, f, K_p). However, calculations have shown that a fixed value of f of 0.003 is adequate for design purposes. Also, experiments indicate that K_p, for a given geometry (A^*, L/D), can be treated as a constant (Fig. 8). This reduces $\Delta P^*/T^*$ to a function of only three parameters, W^*, T^*, and K_m. Moreover, calculations performed with Eq. [12] show the W^* and T^* can be combined as the single term $W^*T^{*0.4}$ for all $T^* \geq 0.3$ with no significant error [Fig. 5 and Table 2, (1)]. This combination has also been verified by experiment (Figs. 4 and 5). These considerations reduce the description of the performance of a particular ejector to a relation between three variables,

$$\frac{\Delta P^*}{T^*} = \phi[W^*T^{*0.4},\ K_m]$$

with a consequent simplification of the ejector model test program and also the design procedure.

The ejector performance Eq. [12], using the $W^*T^{*0.4}$ combination, becomes in approximate form:

$$\frac{\Delta P^*}{T^*} = C_1 - C_2(W^*T^{*0.4})^2 - 2C_3(W^*T^{*0.4}) + \frac{K_p^*}{T^*} \qquad [13]$$

and this equation is valid for $T^* \geq 0.3$. Note that for $T^* = 1$, Eqs. [12] and [13] become identical. The coefficients C_1, C_2, and C_3 are defined for both Eqs. [12] and [13] as follows:

$$\left.\begin{aligned} C_1 &\triangleq 2\left(\frac{A_p}{A_m}\right)\left[1 - \frac{A_p}{A_m}(\beta)\right] \\ C_2 &\triangleq 2\left(\frac{A_p}{A_m}\right)\left[\frac{A_p}{A_m}(\beta) - \frac{1}{A^*}\left(1 - \frac{1}{2A^*(A_p/A_m)}\right)\right] \\ 2C_3 &\triangleq 4\left(\frac{A_p}{A_m}\right)^2(\beta) \end{aligned}\right\} \qquad [13a]$$

with

$$\beta \triangleq \left[K_m + \frac{f}{2}\frac{A_w}{A_m} - \frac{\eta_D}{2}\left(1 - \frac{A_m^2}{A_D^2}\right)\right]$$

From the experimental results:

$$K_m = \phi(W^*, T^*, L/D, A^*)$$

As it was expected that the ratio of momentum fluxes,

$$\frac{(w_s V_s)_1}{(w_p V_p)_1} = \left(\frac{w_s}{w_p}\right)^2 \frac{\rho_p}{\rho_s} \cdot \frac{A_p}{A_s} = \frac{(W^* T^{*0.5})^2}{A^*}$$

was the controlling mixing parameter, it was hypothesized that W^* and T^* could be combined as $W^*T^{*0.5}$ to correlate K_m. The work herein presents experimental results that substantiate this hypothesis(Figs. 6 and 7). Hence.

$$K_m = \phi(W^*T^{*0.5}, L/D, A^*)$$

and with the geometry established:

$$K_m = \phi(W^*T^{*0.5})$$

Experimentally, it was found that K_m varies significantly with $W^*T^{*0.5}$ only for $L/D < 4$. For $L/D \geq 4$, K_m depends essentially on geometry only (Figs. 13, 14, 15, and 16).

It is coincidental that the flow rate-temperature correlation parameter for K_m, $W^*T^{*0.5}$, is nearly the same as the $\Delta P^*/T^*$ correlation parameter, $W^*T^{*0.4}$, as these two parameters originated from two unrelated concepts. The K_m correlation factor was hypothesized on the consideration that the ratio of the secondary to primary momentum flux was the fluid parameter characterizing the momentum transport process in the mixing tube. $W^*T^{*0.5}$ was accepted as the correlation parameter on the basis of the model test results. The choice of $W^*T^{*0.4}$ as the $\Delta P^*/T^*$ correlation parameter resulted from calculations performed with the design equation [12]. It was seen that for $T^* \geq 0.3$, the flow rate and temperature ratios could be combined as $W^*T^{*0.4}$ with no significant

error in $\Delta P^*/T^*$ [see Fig. 5 and Table 2, (1)]. This allowed the replacement of $W^{*2}T^*$ by $(W^*T^{*0.4})^2$ and $W^*(1 + T^*)$ by $2W^*T^{*0.4}$ as in Eq. [13]. Experiments verified this combination as a correlation parameter, Figs. 4 and 5. These combinations of flow rate and temperature ratios serve the important functions of simplifying the model test program, the presentation of the results, and the design procedure.

Ejector Energy Efficiency -- A thermodynamically meaningful definition of ejector efficiency is

$$\eta_E = \frac{[w_s(P_a - P_o)/\rho_s]}{[w_p V_p^2/2g_c]} \qquad [14]$$

This is an expression for the efficacy of conversion of the primary jet kinetic energy to secondary stream flow work. This definition is analogous to the usual pump efficiency comparing the fluid flow work increase to the power input. In terms of the nondimensional parameters, [14] becomes

$$\eta_E = (W^*T^{*0.4})(\Delta P^*/T^*)T^{*0.6} \qquad [15]$$

The maximum value of ejector efficiency is useful for the design problem (see Application to Design). The exact expression for maximum ejector efficiency can be found by substituting the expression for $(\Delta P^*/T^*)$ in terms of $W^*T^{*0.4}$, Eq. [13], into [15], differentiating η_E with respect to $W^*T^{*0.4}$, evaluating the $W^*T^{*0.4}$ necessary for maximum efficiency, and inserting this expression back into [15]. However, this is a cumbersome process, and unnecessary as a good approximation for maximum efficiency can be readily established as follows. From Figs. 3, 4, and 5, and Fig. 16 of (1), $W^*T^{*0.4}$ is seen to be essentially a linear function of $\Delta P^*/T^*$. Hence, η_E will be a maximum when $W^*T^{*0.4}$ equals $(W^*T^{*0.4})_{max}/2$ and $\Delta P^*/T^*$ equals $(\Delta P^*/T^*)_{max}/2$. Also, from [13],

$$(\Delta P^*/T^*)_{max} = C_1 + K_p^*/T^* \qquad [16]$$

Therefore,

$$(\eta_E)_{max} = \frac{1}{4} (W^* T^{*0.4})_{max} (C_1 + K_p^*/T^*) T^{*0.6} \qquad [17]$$

This is the approximate expression for maximum ejector efficiency.

FIGURE 1

SIMPLE EJECTOR WITHOUT A DIFFUSER

Illustrates idealizations regarding the entering velocity and temperature profiles.

FIGURE 2

ALTERNATIVE LOCATIONS FOR THE PRIMARY JET DISCHARGE

Location (c) or (d) gives the best performance and location (b) gives poorer performance. The analysis presented in this work is for throat location (a). Limited test results are reported for locations (b) and (c).

FIGURE 3

EJECTOR PERFORMANCE - INFLUENCE OF DEPARTURES FROM SIMPLE ONE-DIMENSIONAL THEORY

1) $K_m = 1$, $K_p = 1$; simple one-dimensional theory.

2) $K_m > 1$, $K_p = 1$; one-dimensional theory modified for nonuniform momentum rate profile leaving the ejector.

3) $K_m > 1$, $K_p < 1$; one-dimensional theory modified for both nonuniform momentum rate and static pressure profiles leaving the ejector.

FIGURES 4 and 5

EJECTOR PERFORMANCE - COMPARISON OF PREDICTED AND MODEL TEST RESULTS

Shaded area indicates uncertainty in predicted results due only to uncertainty in K_m evaluation. Note also that additional uncertainties exist in the measurements of ΔP^* , T^* , and W^* . See Appendix B for a summary of the uncertainties.

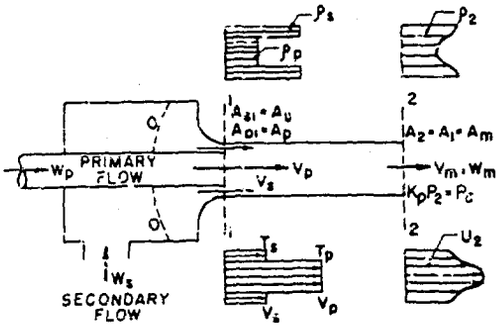

FIG. 1

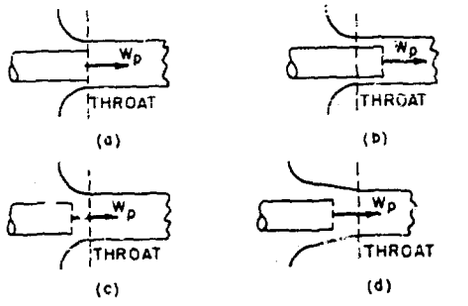

FIG. 2

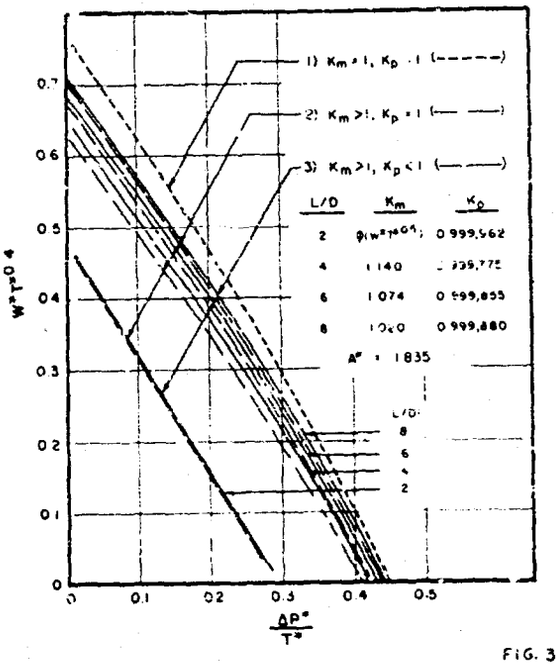

FIG. 3

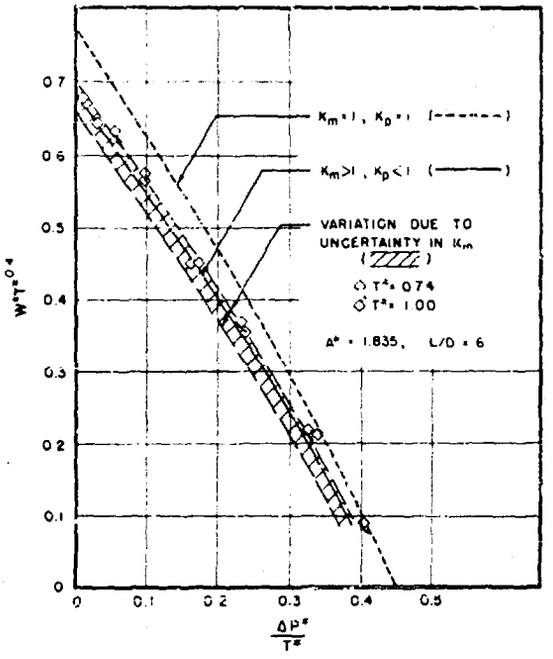

FIG. 4

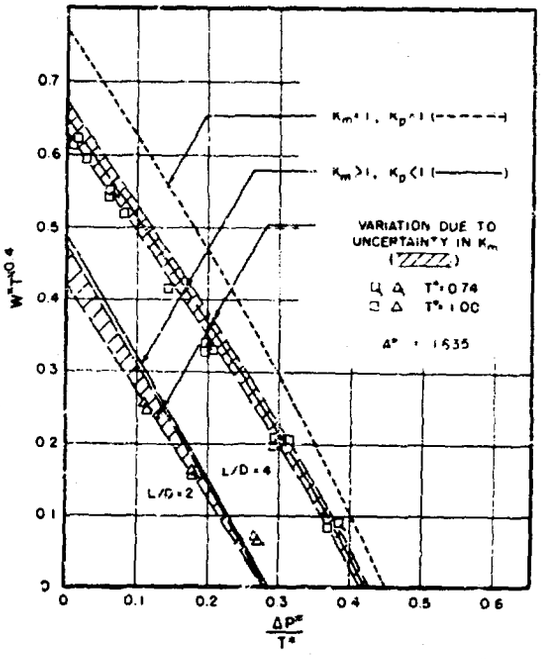

FIG. 5

MODEL TEST RESULTS

K_m Correlation -- One of the primary objectives of this investigation was to determine if $W^*T^{*0.5}$ is an adequate correlating factor for the momentum correction factor K_m. This choice of $W^*T^{*0.5}$ resulted from the intuitive conclusion that the ratio of secondary to primary momentum flux characterized the momentum transport process:

$$\frac{(w_s V_s)_1}{(w_p V_p)_1} = \frac{w_s^2}{w_p^2}\frac{\rho_p}{\rho_s}\frac{A_p}{A_s} = \frac{(W^*T^{*0.5})^2}{A^*}$$

To test this choice, the expression for K_m at $x/D = 0$ and $L/D > 0$, designated $K_{m,o}$, was formulated theoretically, (1), with the idealizations that V_s, V_p, T_s, and T_p are constant across the secondary and primary streams, respectively (idealization 3, page 7):

$$K_{m,o} = \frac{1}{(A_p/A_m)} \frac{1}{(W^*T^* + 1)(W^* + 1)} \left[1 + \frac{W^{*2}T^*}{A^*}\right] \qquad [18]$$

The specification that L/D is greater than zero in evaluating $K_{m,o}$ is necessary to insure that there will be an induced flow. Here, if $(W^*T^* + 1)(W^* + 1)$ is replaced by the approximation $(1 + W^*T^{*0.5})^2$, there is no significant error introduced in $K_{m,o}$ providing $T^* \geq 0.3$, Fig. 23, p. 34, (1). Thus with the ejector geometry specified, $K_{m,o}$ becomes, to a good approximation, a function of $W^*T^{*0.5}$ only, instead of W^* and T^* separately:

$$K_{m,o} = \frac{1}{(A_p/A_m)} \left[\frac{1}{(1 + W^*T^{*0.5})^2}\right]\left[1 + \frac{(W^*T^{*0.5})^2}{A^*}\right] \qquad [19]$$

Another factor influencing the choice of $W^*T^{*0.5}$ is that the dependency of K_m on W^* and T^* decreases as the length (L/D) of the ejector is increased. The maximum dependency of K_m on W^* and T^* occurs at an x/D of zero, and for $x/D \geq 4$, K_m is essentially a function of geometry

alone. This fact makes the acceptance of $W^*T^{*0.5}$ as the combined flow-temperature parameter an even better approximation than suggested above.

To test these considerations, K_m was evaluated at x/D's of 0 and 2 with A*'s of 1.835 and 6.984 (L/D = 8) by integration of the velocity and temperature profiles at these stations in the mixing tube. The resulting K_m's were plotted as functions of both W^* and $W^*T^{*0.5}$ (Figs. 6 and 7). The tests were carried out for temperature ratios of 0.74 and 1.00 . For the x/D = 0 results, the relation between $K_{m,o}$ and $W^*T^{*0.5}$ is Eq. [19] for $T^* \geq 0.3$. The standard deviations of the data about $K_{m,o}$ for K_m as a function of $W^*T^{*0.5}$ and for K_m as a function of W^* were determined. As no analytical prediction exists for K_m at x/D = 2 , least-square straight lines were drawn through the data for K_m as a function of $W^*T^{*0.5}$ and for K_m as a function of W^* . (The experimental results indicate that K_m is nearly linear with $W^*T^{*0.5}$ for $x/D \geq 2$.) The standard deviations of the data about these lines were also determined. The resulting values of the relative standard deviations $(\sigma_{W^*}/\sigma_{W^*T^*0.5})$ are:

	A* = 1.835	A* = 6.984
x/D = 0	2.1	3.6
x/D = 2	10.7	5.2

As the correlation of K_m with $W^*T^{*0.5}$ reduces the spread of the data by factors of 2:1 to 10:1, $W^*T^{*0.5}$ is definitely acceptable. However, additional confirmation at test magnitudes down to $T^* \simeq 0.3$ would be desirable.

<u>$\Delta P^*/T^*$ Correlation</u> -- The flow rate-temperature correlating parameter for $\Delta P^*/T^*$ is $W^*T^{*0.4}$. This choice was based on calculations with the ejector design equation [12] which demonstrated that W^* and T^* could be combined as $W^*T^{*0.4}$ for all $T^* \geq 0.3$ with no significant change in the value of $\Delta P^*/T^*$ [(1), Fig. 5 and Table 4]. The results

of the model tests substantiate this conclusion (Figs. 4 and 5). The values of $\Delta P^*/T^*$ for $T^* = 0.74$ are consistently in agreement with those for $T^* = 1.00$; thus $W^*T^{*0.4}$ is verified as the $\Delta P^*/T^*$ correlation parameter.

K_m Design Results -- In (1) and (2) and in the early stages of this work, the momentum correction factor, K_m , was evaluated by integration of the velocity and temperature profiles across the mixing tube. The profiles were determined by Pitot tube velocity and thermocouple temperature traverses. As a check on the accuracy of the traverse results, the metered incoming primary and secondary flow rates were compared to those obtained by the integration of the profiles. The results obtained by integration were consistently higher than the metered results. This error may well be attributed to the high turbulent velocity fluctuations in the mixing regions; Corrisin (4) found velocity fluctuation values of u'/U_{local} of 0.1 to 0.5 in the mixing region of a free jet. The velocity fluctuations simulate a more even distribution of momentum flux than actually exists in the mixing region (see Appendix B for an analysis of the effect of the turbulent velocity fluctuations on K_m). As a result, the K_m values obtained from the velocity and temperature profiles are lower than the actual K_m's.

The K_m uncertainty due to this effect and instrument uncertainty is estimated to be only $\pm$ 2% for $x/D \geq 4$, but for $x/D < 4$, K_m is estimated to be 1 to 5% too low. As a consequence the resulting uncertainties in the predicted values of $\Delta P^*/T^*$ are 2 to 15 per cent (see Figs. 4 and 5).

The uncertainty in $\Delta P^*/T^*$ is $\pm$ 3% when $\Delta P^*/T^*$ is measured directly. As this is generally less than the uncertainty in $\Delta P^*/T^*$ resulting from the K_m traverse results, it was concluded that K_m calculated directly from the measured $\Delta P^*/T^*$ using Eq. [11] would provide the best K_m data for design purposes. The uncertainty of K_m by this procedure is estimated to be about $\pm$ 1%.

Another reason for calculating K_m from Eq. [11]

is that the length of the mixing tube influences the velocity and temperature profiles at positions along the mixing tube. In (1), all K_m values were computed by integration of the velocity and temperature profiles at stations along a mixing tube of length $L/D = 8$. The K_m's obtained at positions along a long mixing tube are higher than the K_m's determined at the discharge of a short mixing tube (see Fig. 7 for a comparison of K_m at $x/D = 2$ evaluated from traverses for L/D's of 8 and 2 respectively). This difference is attributed to a difference in flow patterns -- separation is present at $x/D = 2$ in the long mixing tube, but is not when the mixing tube length is $L/D = 2$. These difficulties are circumvented when K_m is evaluated from the design equation and the experimentally determined $\Delta P^*/T^*$.

The K_m results presented in Figs. 13, 14, and 15 have been derived directly from $\Delta P^*/T^*$ measurements as described above. The $L/D \geq 4$ results are unaffected by the aforementioned changes; consequently Fig. 16 is taken directly from (1).

These K_m results are improved over those presented previously (1) in that: a) the K_m values have been improved by use of the new computing technique, and b) the results for $L/D = 1$, 2, and 3 have been extended from an A^* range of 1 to 4 to a range of 1 to 7.

K_p Design Results -- The K_p factor is needed to account for the conversion of kinetic energy to flow work that occurs after the ejector has exhausted to the atmosphere. Even though this process occurs outside the ejector, it affects the performance in that the mean exit static pressure of the ejector is slightly less than atmospheric. This diffusing action is generally small but produces up to a 20 per cent increase in performance in $\Delta P^*/T^*$ at high mignitudes of $W^*T^{*0.4}$ and also in $W^*T^{*0.4}$ at high magnitudes of $\Delta P^*/T^*$. These effects are evident in Fig. 3.

The variation of K_p with W^* is plotted in Fig. 8 for

$A^* = 1.835$. L/D was taken as the dependent variable and W^* was omitted as the variation in K_p is slight, and as $\Delta P^*/T^*$ does not depend markedly on K_p . It is seen from Eq. [13] that a change of 20 per cent in $(1 - K_p)$ produces only a 2 per cent change in $\Delta P^*/T^*$. The variation of K_p with L/D for A^*'s of 1.835, 3.741, and 6.984 is presented in Figs. 9, 10, and 11. Figure 12 is the cross-plotted relation between K_p and A^* providing the design curve to accompany Figs. 13 to 16 for K_m .

Nozzle Location Results -- Some limited results are presented for the ejector configuration with the primary nozzle discharge displaced from the throat of the secondary nozzle (see Fig. 2c). The one geometry tested was $A^* = 1.835$ and $L/D = 8$. Figure 18 presents the variation of $W^*T^{*0.4}$ with $\Delta P^*/T^*$. At a given $\Delta P^*/T^*$ the flow rate is increased about 10 per cent at the low values of $\Delta P^*/T^*$ and 2 per cent at the high values. The maximum increases occur when the nozzle is one mixing tube diameter into the plenum chamber $[(x/D)_n = -1]$ at low $\Delta P^*/T^*$ and at $(x/D)_n = -0.25$ at high $\Delta P^*/T^*$'s . The variation of $W^*T^{*0.4}$ with $(x/D)_n$ for constant $\Delta P^*/T^*$ is presented in Fig. 19. The curves are quite flat, indicating that the position of the primary nozzle is not too critical. The upstream position for optimum performance is seen to decrease as $W^*T^{*0.4}$ decreases.

This behavior may be explained by the fact that the angle at which the jet spreads is proportional to $(V_p - V_s)/(V_p + V_s)$ (5). Decreasing W^* increases $(V_p - V_s)/(V_p + V_s)$; the jet spreads faster at low W^* . If the primary nozzle is too far into the plenum chamber, the primary jet will be diverted into the plenum chamber by the secondary nozzle walls.

The fact that an improvement in $W^*T^{*0.4}$ occurs by displacing the primary nozzle discharge into the plenum chamber can be rationalized with the help of the momentum relation. With the primary nozzle in the plenum chamber, the incoming momentum rate is $K_{m,1}[(W_m V_m)/g_c]$ instead of

$[(w_p V_p)/g_c] + [(w_s V_s)/g_c]$. Equation [3] becomes

$$K_{m,1}\left[\frac{w_m V_m}{g_c}\right] + P_1 A_1 = K_m\left[\frac{w_m V_m}{g_c}\right] + (K_p P_2)A_2 - F_{fr} \qquad [3b]$$

or

$$(K_p P_2 - P_1)A_1 = (K_{m,1} - K_m)\left[\frac{W_m V_m}{g_c}\right] - F_{fr} \qquad [3c]$$

Now, as some mixing has taken place between the nozzle discharge and section 1, $K_{m,1}$ is less than $K_{m,o}$; Eq. [3] could be written with $K_{m,o}[(w_m V_m)/g_c]$ instead of $[(w_p V_p)/g_c] + [(w_s V_s)/g_c]$. Hence, for the same $\Delta P^*/T^*$, which is proportional to $(K_p P_2 - P_1)$, $W^* T^{*0.4}$ must increase. While this effect should be investigated further, a tentative conclusion is that a performance gain of about 10 per cent may be obtained by moving the primary nozzle about one mixing tube diameter into the plenum chamber.

An investigation of the influence of the shape of the secondary flow nozzle together with primary nozzle location may demonstrate that even greater improvements in performance are possible, (see Fig. 2d).

FIGURE 6

K_m AS A FUNCTION OF W^* AND $W^*T^{*0.5}$

Demonstrates correlation provided by combining W^* and T^* in the form $W^*T^{*0.5}$. $K_{m,o}$ is derived theoretically from the idealizations of uniform flow velocity and temperature of both the primary and secondary streams at Section 1.

FIGURE 7

K_m AS A FUNCTION OF $W^*T^{*0.5}$

Demonstrates correlation provided by combining W^* and T^* in the form $W^*T^{*0.5}$. Also illustrates the influence of overall length of the mixing tube at $x/D = 2$, where $L/D = 2$ is compared to $L/D = 8$. The $x/D = 0$ line is the analytical derived relation equation [19]. The $x/D = 2$ line is based on experiments with $T^* = 1$.

FIGURE 8

K_p AS A FUNCTION OF W^*

Illustrates the influence of L/D. The results are obtained from integration of the static pressure profiles.

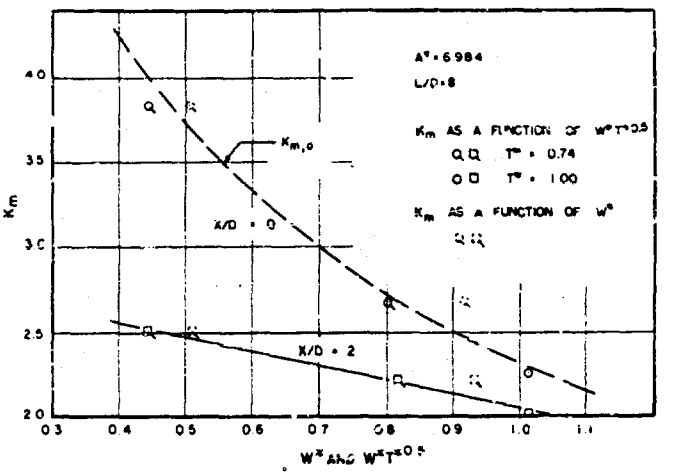

FIG. 6

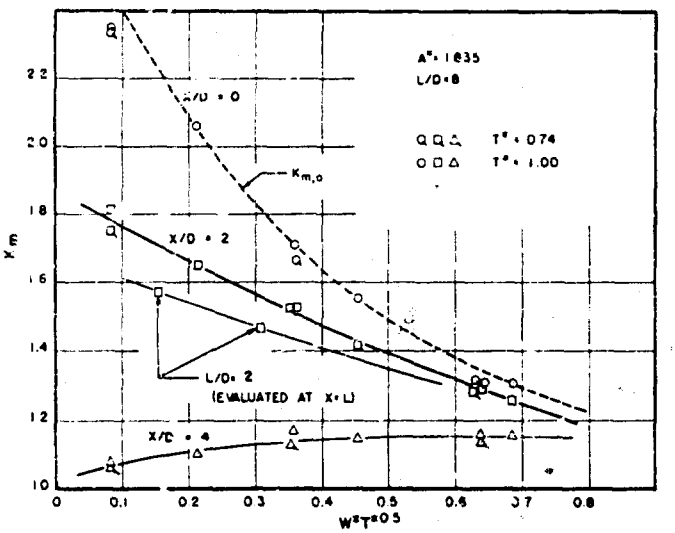

FIG. 7

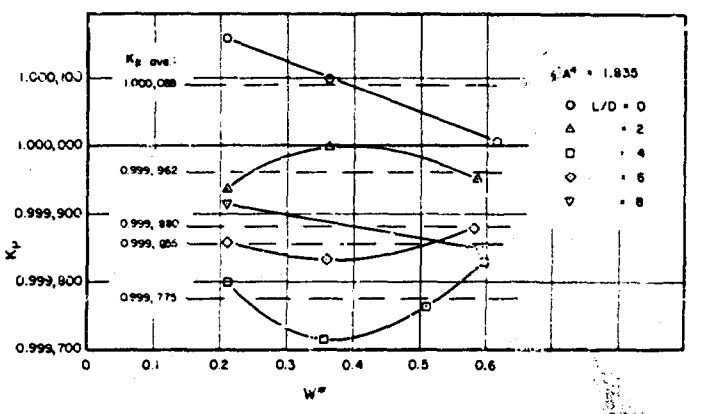

FIG. 8

FIGURES 9, 10, and 11

K_p AS A FUNCTION OF L/D

See Page 23 for the effect of using the average value of K_p in the design equation [13].

FIGURE 12

K_p DESIGN RESULTS

Curves are cross-plotted from Figs. 9, 10, and 11.

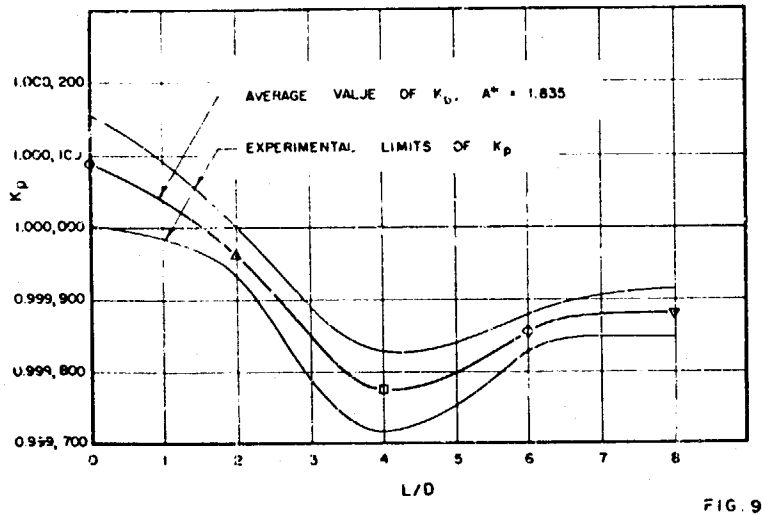

FIG. 9

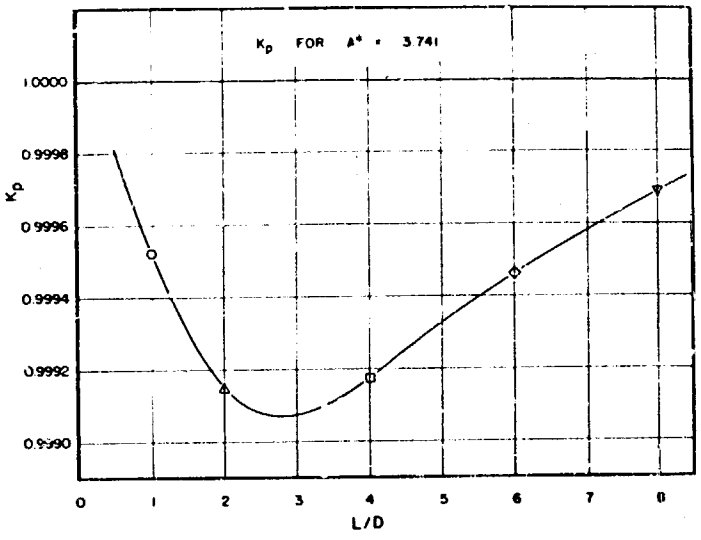

FIG. 10

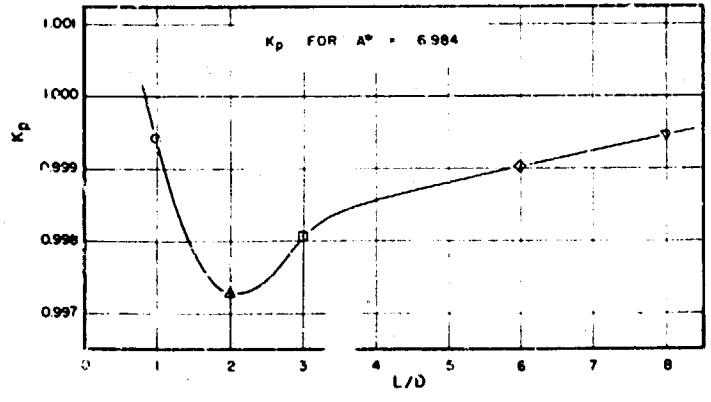

FIG. 11

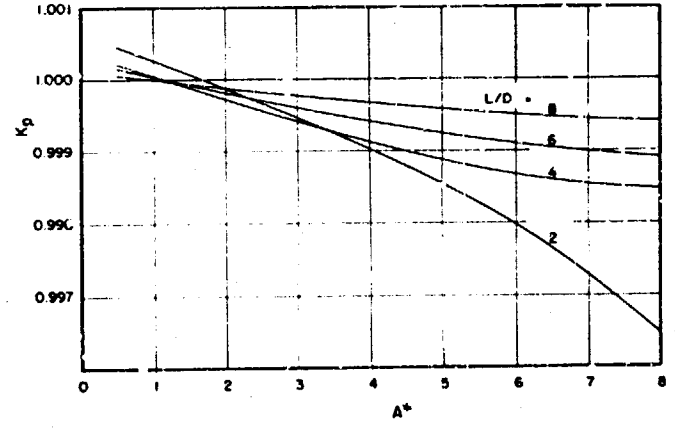

FIG. 12

FIGURES 13, 14, 15, and 16

K_m DESIGN RESULTS

Figures 13, 14, and 15 are to be used in place of Figs. 18, 19, and 20 of TR-No. 26 (1). Figure 16 is Fig. 21 of TR-No. 26.

FIGURE 17

MAXIMUM $W^*T^{*0.4}$ AS A FUNCTION OF A^* , $\Delta P^*/T^* = 0$

The values are computed from the design equation [13] and from Figs. 13, 14, 15 and 16.

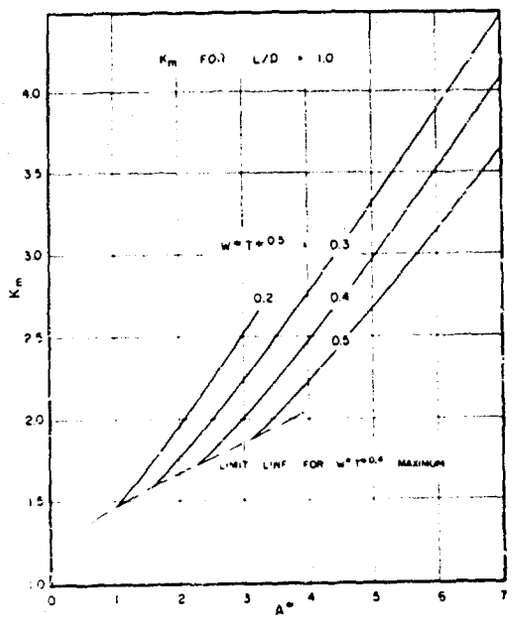

FIG. 13

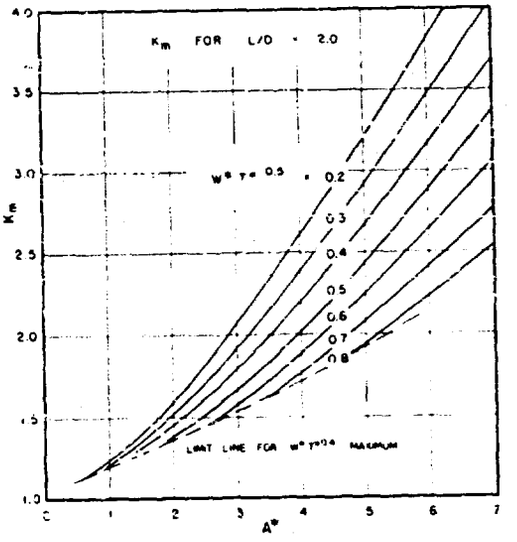

FIG. 14

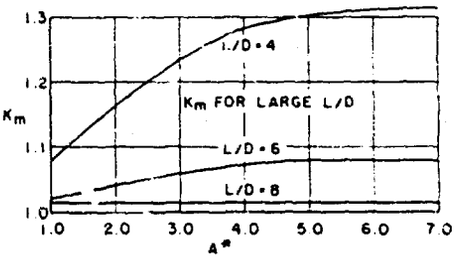

FIG. 16

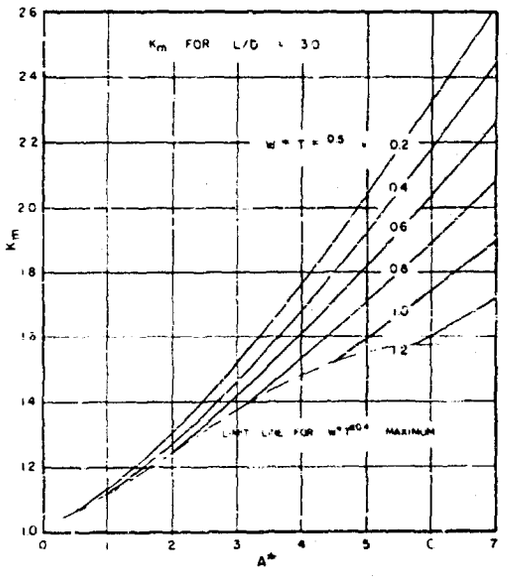

FIG. 15

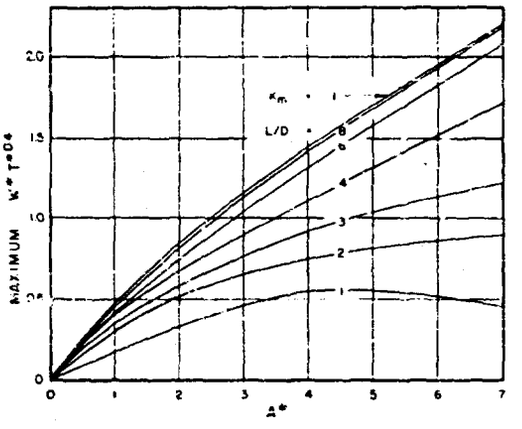

FIG. 17

FIGURE 18

EJECTOR PERFORMANCE FOR THE PRIMARY NOZZLE DISPLACED FROM THE THROAT OF THE SECONDARY NOZZLE

FIGURE 19

$W^*T^{*0.4}$ AS A FUNCTION OF PRIMARY NOZZLE POSITION, $(x/D)_p$ FOR CONSTANT $\Delta P^*/T^*$

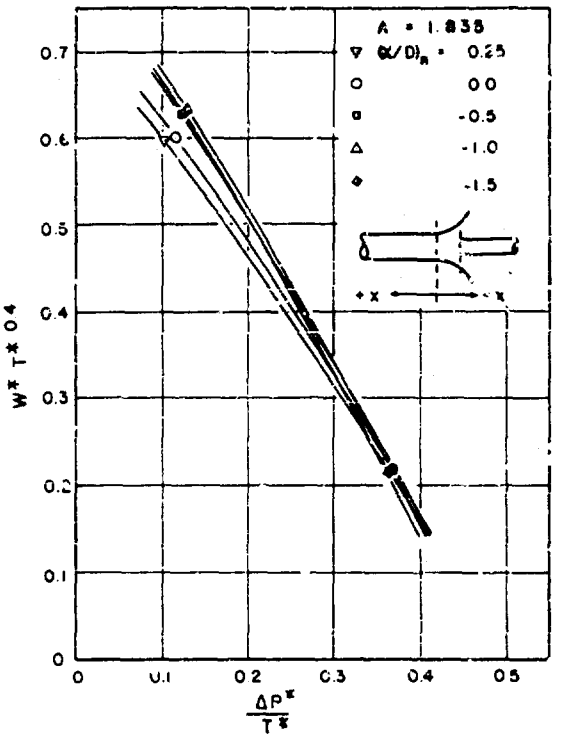

FIG. 18

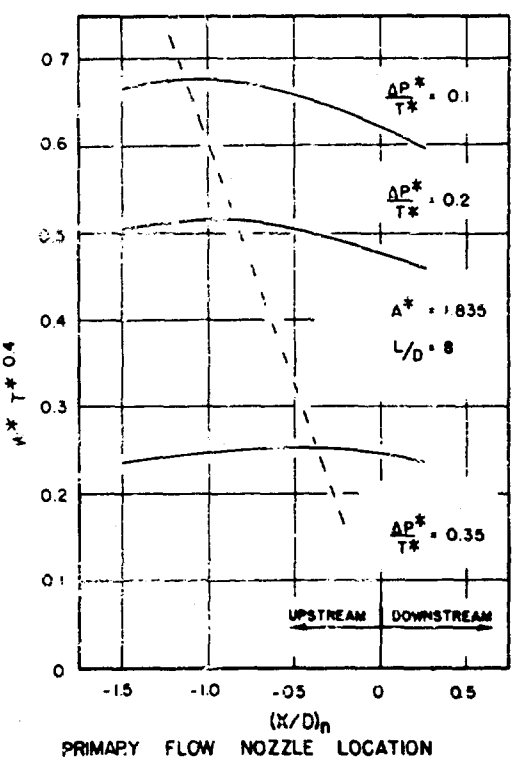

PRIMARY FLOW NOZZLE LOCATION

FIG. 19

APPLICATION TO DESIGN

The information presented in this work enables the designer to define the geometry of a simple jet ejector assuring delivery of a specified secondary flow under specified operating conditions. The design is formulated as follows:

1. The design point specifications of the ejector are first listed. These include the primary flow temperature, mass flow rate, flow area, density, and exit pressure. These quantities will be fixed by the source of the primary stream, probably the exhaust of a prime mover. Additionally, the desired secondary air flow mass rate and temperature will have to be established from the cooling or ventilating requirements. An estimate of the pressure rise for the ejector is also required; this estimate is determined by the ejector exit pressure relative to the minimum plenum chamber pressure.

2. From the values of the flow rate and temperature specifications, w_s, w_p, T_s, and T_p, and the estimated pressure rise, listed under step 1, the nondimensional performance parameters, $(W^*T^{*0.4})_{d.p.}$ and $(\Delta P^*/T^*)_{d.p.}$, at the design point are computed.

3. The value of $(W^*T^{*0.4})_{max}$ is now computed by doubling $(W^*T^{*0.4})_{d.p.}$ (see Analysis). Figure 17 is entered with this value, and the compatible geometries (L/D and A*) are listed. The values of $(\Delta P^*/T^*)_{max}$ corresponding to these geometries are evaluated using Eq. [16]; C_1 is defined by the equation set [13a], the values of K_m are taken from the appropriate Figs. 13, 14, 15 or 16, and the values of K_p from Fig. 12. The values of $(\Delta P^*/T^*)_{max}$ and the value of $(W^*T^{*0.4})_{max}$ are entered on a design plot of $W^*T^{*0.4}$ as a function of $\Delta P^*/T^*$, as in Fig. 20. The design characteristics for the various geometries are then approximated as linear relationships between $W^*T^{*0.4}$ and $\Delta P^*/T^*$. The design point determined in step 2 is entered on the design plot. The geometry of the ejector that will yield the desired performance is defined by the design

characteristic that passes through the design point. (This procedure will yield a design with a slightly higher value of $\Delta P^*/T^*$ than the design value due to the actual slight convex up curvature of the operating characteristic.)

4. With the geometry determined, a more accurate operating characteristic is established with the aid of Eqs. [13] and [13a], Fig. 12, and the pertinent Figs. 13, 14, 15, or 16. The operating point, determined by the intersection of the line of constant $(W^*T^{*0.4})_{d.p.}$ and the operating characteristic, is noted on the design plot, and the corresponding values of $(\Delta P^*/T^*)_{o.p.}$ and η_E are computed.

In order to illustrate the above design method, a sample design will be carried out for the gas turbine installation described in Table 1, (1).

1. Primary and secondary flow specifications:

Primary flow rate	$w_p = 7.00$ lb/sec
Primary flow temperature	$T_p = 1660$ R
Exhaust back pressure	$P_p = 14.7$ psia = 1 atm
Primary flow area	$A_p = 1.07$ ft^2
Primary flow density	$\rho_p = 0.0239$ lb/ft^3
Primary flow velocity	$V_p = 274$ ft/sec
Secondary flow rate	$w_s = 3.50$ lb/sec
Secondary flow temperature	$T_s = 590$ R
Secondary flow density	$\rho_s = 0.0672$ lb/ft^2
Desired minimum ejector pressure rise	$\Delta P = 1"H_2O = 5.20$ #/ft^2

2. Design point values:

$$(W^*T^{*0.4})_{d.p.} = \left(\frac{w_s}{w_p}\right)\left(\frac{T_s}{T_p}\right)^{0.4} = 0.330$$

$$(\Delta P^*/T^*)_{d.p.} = \frac{(\Delta P/\rho_s)}{(V_p^2/2g_c)}\left(\frac{T_p}{T_s}\right) = 0.187$$

3. The geometries that will deliver the required $(W^*T^{*0.4})_{max} = 2(W^*T^{*0.4})_{d.p.} = 0.660$, and the values of $(\Delta P^*/T^*)_{max}$ associated with these geometries, are presented in Table I. The design curves corresponding to these geometries are plotted on Fig. 20. The design curve that falls closest to the design point is curve b); the geometrical constants are $L/D = 3$ and $A^* = 2.31$. The operating characteristics can now be determined more accurately using Eq.[13];as K_m is a function of $W^*T^{*0.5}$ Fig.1 is also used.

4. The data needed to establish the operating characteristic is presented in Table II. The resulting ejector operating characteristic is shown on the design plot. It is seen that the operating point occurs at a slightly higher $\Delta P^*/T^*$ than the design point value. The operating point values are:

$$(W^*T^{*0.4})_{o.p.} = 0.330$$

$$(\Delta P^*/T^*)_{o.p.} = 0.197$$

The ejector operating efficiency, computed from Eq. [15], is:

$$\eta_E = 3.5 \text{ per cent}$$

The above design procedure defines the ejector of minimum length ($L/D = 3$, $A^* = 2.31$) that will provide the desired performance. If a longer ejector is allowable, and a conservative design is desired, a design curve such as c) of Fig. 20 may be chosen ($L/D = 4$, $A^* = 1.88$). The operating condition will now deliver the same $W^*T^{*0.4}$ at a higher value of $\Delta P^*/T^*$; alternatively, a higher $W^*T^{*0.4}$ at the design point value of $\Delta P^*/T^*$ may be obtained.

As previously mentioned, the concept of ejector efficiency is useful and thermodynamically meaningful in that it provides a basis of comparison between the ejector and the conventional fluid pump. The ejector definitely suffers efficiency-wise in comparison, as can be seen in Fig. 21 where $\eta_{E\ max}/T^{*0.6}$ as a function of A^* for various L/D's is presented. The

maximum efficiency realizable for the ejector characteristics presented in this work is about 12 per cent. While the efficiency is low, it is acceptable if the ejector exploits energy that would otherwise be wasted. The ejector eliminates the initial cost, weight, and power requirements of the blowers that would be used. Also, an increase in plant thermal efficiency is realized by the reduction in exhaust back pressure. For a gas turbine plant, these considerations can result in a net saving of one to one and one-half per cent on fuel consumption, (1).

TABLE I

Design curve calculations for sample design

Curve	L/D	A*	K_m	C_1	K_p	K_p^*/T^*	$(\Delta P^*/T^*)_{max}$
a)	2	2.97	2.08*	0.238	0.99945	0.041	0.279
b)	3	2.31	1.37*	0.350	0.99970	0.022	0.372
c)	4	1.88	1.15	0.412	0.99975	0.019	0.431
d)	6	1.69	1.03	0.447	0.99990	0.007	0.454
e)	8	1.53	1.015	0.459	0.99995	0.004	0.463

*As K_m for $W^*T^{*0.4} = 0$ is not evaluated for these geometries, a value for K_m slightly higher than that for $W^*T^{*0.5} = 0.2$ is chosen from Figs. 14 and 15.

TABLE II

Operating characteristic calculations for sample design

$W^*T^{*0.4}$	$W^*T^{*0.5}$	K_m	β	C_1	C_2	$2C_3$	$\Delta P^*/T^*$
0	0	1.38	1.40	0.350	-	-	0.372
0.222	0.2	1.37	1.39	0.352	0.178	0.504	0.253
0.333	0.3	1.35	1.37	0.354	0.176	0.500	0.189
0.444	0.4	1.32	1.34	0.360	0.170	0.489	0.121
0.660	-	-	-	-	-	-	0

FIGURE 20

DESIGN AND OPERATING CHARACTERISTIC CURVES

The graphical results for the sample design calculations.

FIGURE 21

MAXIMUM EJECTOR EFFICIENCY AS A FUNCTION OF GEOMETRY

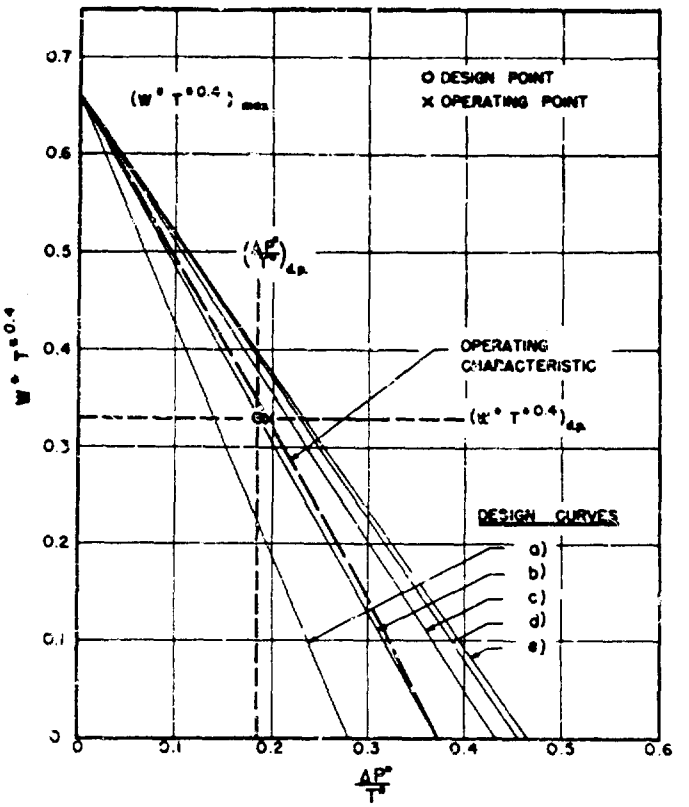
O DESIGN POINT
× OPERATING POINT
$(W^* T^{*0.4})_{max}$
$(\frac{\Delta P^*}{T^*})_{d.p.}$
OPERATING CHARACTERISTIC
$(W^* T^{*0.4})_{d.p.}$
DESIGN CURVES
a)
b)
c)
d)
e)
$W^* T^{*0.4}$
$\frac{\Delta P^*}{T^*}$
0.7
0.6
0.5
0.4
0.3
0.2
0.1
0
0.1
0.2
0.3
0.4
0.5
0.6

FIG. 20

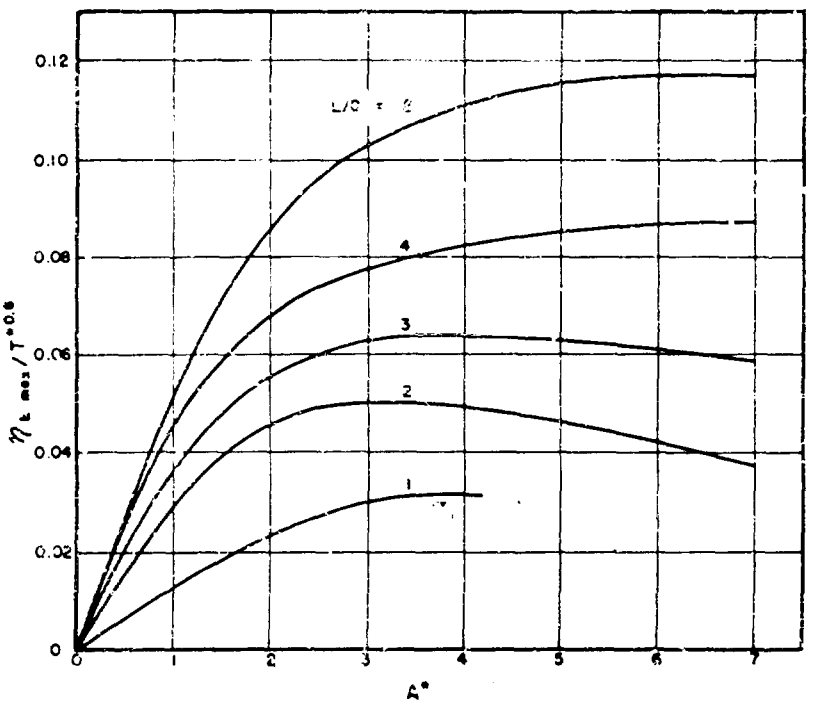
L/D = 2
4
3
2
1
$\eta_{t\,max}/T^{*0.6}$
A^*
0.12
0.10
0.08
0.06
0.04
0.02
0
1
2
3
4
5
6
7

FIG. 21

APPENDIX A
VELOCITY AND TEMPERATURE TRAVERSE RESULTS

Velocity and Temperature Profiles -- Some typical ejector velocity and temperature profiles are presented in Figs. 22 and 23. Figure 22 illustrates the profile development at stations along the mixing tube; the data points were obtained from averages on either side of the tube centerline. The $x/D = 0$ profiles approximate quite closely the idealized entering profiles. The temperature profile at $x/D = 0$ is less sharply divided into two regions due to heat transfer from the primary stream through the copper nozzle to the secondary stream. Although this effect is more noticeable at low flow rate ratios, the influence on K_m is always small, the measured K_m being within 5 per cent of the values reported. The presence of inflection points indicates that the profiles are far from established at $x/D = 4$, a result verified by the high K_m at this station (Fig. 16).

Figure 23 describes the good flow symmetry found in the ejector at an x/D of 2 by superimposing the data points taken on either side of the tube centerline. The asymmetry, caused by nonuniform entrainment and mixing, is seen to be negligible for the temperature distribution; the disagreement between temperatures on either side of the centerline is about one per cent of full scale. The velocity distribution is more asymmetric; the difference is about five per cent of full scale. These profiles represent the maximum asymmetry, occurring at low $W^*T^{*0.5}$ and an x/D of 2. The profiles also illustrate the flow separation at the wall occurring for large L/D at x/D's of 1, 2, and 3 for low $W^*T^{*0.5}$; $U/U_{\mathfrak{L}}$ is negative for $0.9 < r/r_o \leq 1.0$. The separation region is stable, and occupies up to 20 per cent of the mixing tube cross-sectional area. As stated previously, separation is not present for $x/D \equiv L/D = 1$, 2, or 3.

Diffusion of Momentum and Temperature -- An examination of the temperature and velocity profiles reveals that temperature

spreads faster than momentum (Figs. 22 and 23). This conclusion is confirmed by the work of Landis and Shapiro (9); however, the statement that the profiles are similar is not confirmed. In Fig. 23, the temperature is nearly uniform across the tube while the velocity variation is great and separation occurs at the wall. This disagreement results from a major difference in system geometry. The results of (9) were taken on an ejector with an area ratio of 63, while the present ejector has an area ratio of 1.835. The results of (9) are to be interpreted as approximating the mixing characteristics of a jet discharging into an infinite flowing medium, and not those of low area ratio ejectors.

The centerline decay results (Fig. 24) are compatible with the experimental results of (9), curves b) and c), and with the established correlation for free jet discharge into a medium at rest, curve a). The trend is one of increasing decay of centerline velocity with decreasing $W^*T^{*0.5}$. The established empirical correlation for centerline velocity decay for jets discharging into an infinite flowing medium is given in (10) as:

$$\frac{U_{\ell} - V_s}{V_p - V_s} = \frac{L}{x/D_n} \quad , \quad \text{for} \quad x/D_n > L$$

where L, the length of the potential core region, is given by

$$L = 4 + 12\lambda$$

and

$$\lambda \triangleq V_s/V_p$$

$$x/D_n = \text{flow length/primary nozzle diameter}$$

Attempts to use this correlation to predict the present ejector behavior are also shown on Fig. 24. The agreement between the data points for $x/D_n = 6.6$ and the prediction indicates that the correlation, for $T^* = 1.00$, may hold for low area ratio ejectors. However, as data points with different λ,

but equal $W^*T^{*0.5}$, have the same centerline decay, λ is not the only parameter governing the centerline velocity decay. In terms of the present nomenclature, λ can be expressed as:

$$\lambda \triangleq \frac{V_s}{V_p} = \frac{w_s}{\rho_s A_s} \cdot \frac{A_p \rho_p}{w_s} = \frac{W^* T^*}{A^*}$$

or

$$\lambda / T^{*0.5} = \frac{W^* T^{*0.5}}{A^*}$$

In view of the present experimental results, it seems probable that $\lambda/T^{*0.5}$, rather than λ, should be used in the correlation. However, more data is needed to definitely confirm this choice.

The centerline temperature decay results, Fig. 25, do not follow the trends of (9) as closely as the velocity decay results do. The behavior is similar in that the decay increases as the value of λ, and $W^*T^{*0.5}$ decreases, but the lack of enough data precludes a meaningful comparison. The difference in geometry influences the centerline decay also.

The existing centerline decay correlations, such as from (9), are derived mainly from high area ratio ejectors and are not suitable for low area ratio ejectors as these correlations require that the centerline values approach the secondary stream values as x/D_n becomes very large. For high area ratio ejectors, this is a fairly good approximation as can be demonstrated by the following considerations. For all ejectors, the flow at large x/D_n approaches fully established turbulent pipe flow and the centerline velocity approaches within 20 per cent the bulk average velocity ($U_{\mathfrak{L}} > V_m$ always). V_m is essentially equal to V_s if the primary area is small compared to the secondary area (large A^*). Also for fully established, low velocity, adiabatic flow, the centerline temperature is equal to the bulk average temperature, and T_m is essentially equal to T_s if A^* is large so that the primary

flow rate is small compared to the secondary flow rate. For low area ratios, and therefore low flow rate ratios, this is not true; the bulk average quantities are considerably different from the secondary quantities, and the temperature and velocity decay parameters will not tend to zero as x/D_n increases. This can easily be seen by formulating the bulk average velocity and temperature, normalized by V_p and T_p respectively, in terms of the present nomenclature:

$$\frac{V_m}{V_p} = \frac{(w_p + w_s)}{(A_p + A_s)\rho_m} \cdot \frac{\rho_p A_p}{w_p} = \frac{(1 + W^*)}{(1 + A^*)} \cdot \frac{T_m}{T_p}$$

$$\frac{T_m}{T_p} = \frac{w_p}{(w_p + w_s)} \cdot \frac{T_p}{T_p} + \frac{w_s}{(w_p + w_s)} \cdot \frac{T_s}{T_p} = \frac{(1 + W^*T^*)}{(1 + W^*)}$$

The limiting values of the nondimensional parameters used to correlate the centerline decays can now be formed. The fully established value of $U_{\mathfrak{L}}$ is assumed to be $1.2V_m$; the fully established value of $T_{\mathfrak{L}}$ is T_m .

$$\frac{U_{\mathfrak{L}} - V_s}{V_p - V_s} = \frac{1}{1 + A^*}\left[1 + 0.2A^* \frac{(1 + W^*T^*)}{(A^* - W^*T^*)}\right]$$

$$\frac{T_{\mathfrak{L}} - T_s}{T_p - T_s} = \frac{1}{1 + W^*}$$

For the large area ratio ejector, as in (9), these limits are relatively close to zero; for $A^* = 63$ and $W^*T^{*0.5} = 36$,

$$\frac{U_{\mathfrak{L}} - V_s}{V_p - V_s} = 0.28 \quad \text{and} \quad \frac{T_{\mathfrak{L}} - T_s}{T_p - T_s} = 0.027$$

However, for low area ratio ejectors, these limits are considerably different from zero; for $A^* = 1.835$ and $W^*T^{*0.5} = 0.64$,

$$\frac{U_{\ell} - V_s}{V_p - V_s} = 0.53 \qquad \text{and} \qquad \frac{T_{\ell} - T_s}{T_p - T_s} = 0.61$$

The conclusions and recommendations that can be drawn from this discussion are:

1. Further investigations of the temperature and momentum profiles are needed to establish the mixing profiles of low area ratio ejectors and to establish the correspondence between low and high area ratio ejectors.

2. More data is needed to ascertain if the empirical correlation presented in (10) for the centerline velocity decay is valid for low area ratio ejectors for even a limited region, and whether $\lambda/T^{*0.5}$ is a better correlating parameter than λ for centerline decay. It is also necessary to investigate the importance of the bulk average properties, and to determine whether these properties can profitably be used in establishing a correlation.

To this end it is recommended that data be taken of the centerline velocity and temperatures over a range of A^* and T^* magnitudes. These results should provide a test for the validity of the proposed $\lambda/T^{*0.5}$ correlating parameter. It also seems probable that the velocity decay should be expressed as

$$\frac{(U_{\ell} - V_m)}{(V_p - V_m)} \qquad \text{rather than} \qquad \frac{(U_{\ell} - V_s)}{(V_p - V_s)}$$

and similar ratios for temperature. Then both the low and high A^* geometries would have common asymptotic magnitudes for large x/D_n .

FIGURE 22

VELOCITY AND TEMPERATURE PROFILES

Illustrates development of the profiles at stations along the mixing tube.

FIGURE 23

VELOCITY AND TEMPERATURE PROFILES AT A LOW x/D AND $W^*T^{*0.5}$

Illustrates the asymmetry and separation present.

FIGURE 24

CENTERLINE VELOCITY DECAY

FIGURE 25

CENTERLINE TEMPERATURE DECAY

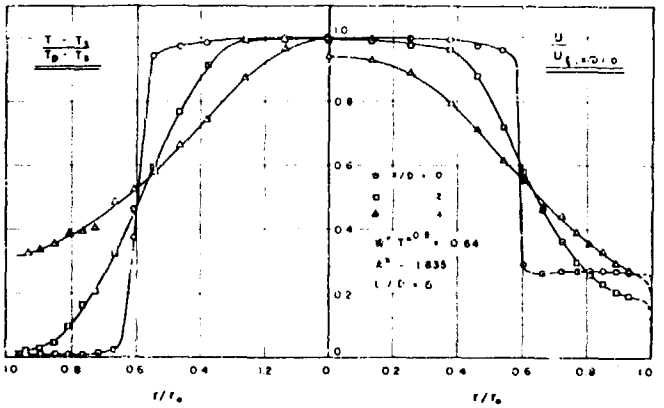

FIG. 22

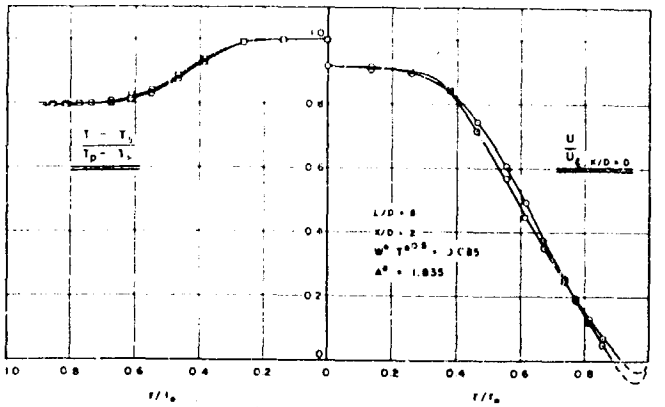

FIG. 23

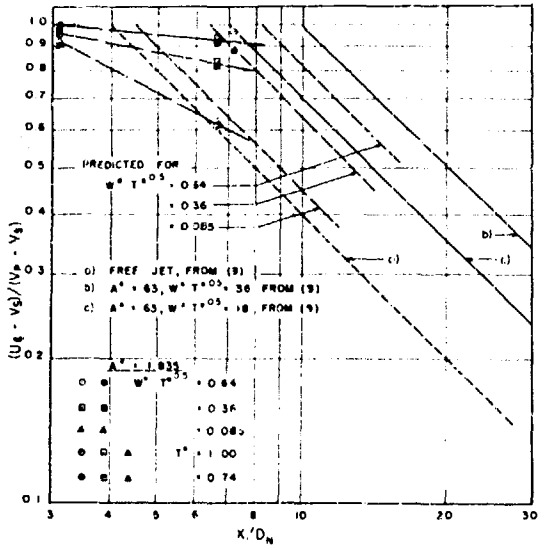

FIG 24

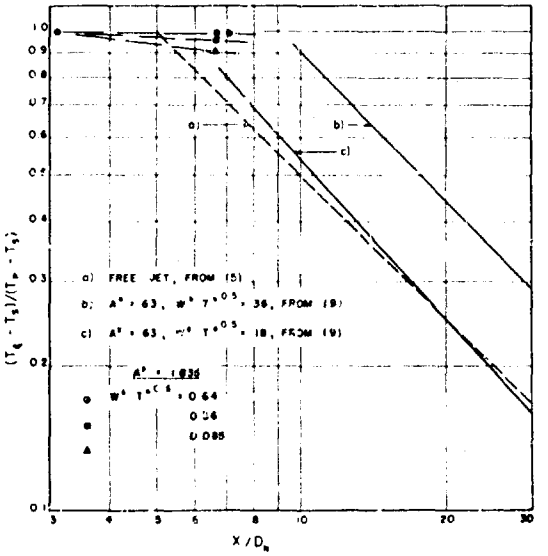

FIG 25

APPENDIX B
ANALYSIS OF EXPERIMENTAL UNCERTAINTIES

The estimated experimental uncertainties of the main test results are as follows:

Quantity	Uncertainty
W^*	$\pm$ 1.2%
T^*	$\pm$ 0.1%
$W^*T^{*0.5}$ and $W^*T^{*0.4}$	$\pm$ 1.2%
$\Delta P^*/T^*$	$\pm$ 3.1%
K_m (from $\Delta P^*/T^*$)	$\pm$ 1 %
K_m ($x/D \geq 4$, traverse)	$\pm$ 2 %
K_m ($x/D \leq 4$, traverse)	+1 to +5%

The K_m's evaluated from the velocity and temperature traverses have higher uncertainties compared to the evaluations from overall ejector performance as the highly turbulent and rotational flow in the mixing regions produce large uncertainties in the profiles (a discussion of these effects follows in Appendix C). The uncertainty due to these fluctuations is determined by the following observations.

The pitot tube readings are too high due to turbulent velocity fluctuations; the velocity profiles computed from these readings will be too high also. As the velocity gradient is greatest between $x/D = 0$ and $x/D = 4$, the fluctuations will be highest here. This is evidenced in that the discrepancy between metered and integrated flow rates is a maximum at $x/D = 2$, and negligible at $x/D = 6$ and 8. A crude analysis of the effect of these fluctuations was undertaken on Run 51 ($W^* = 0.73$, $x/D = 2$), Run 64 ($W^* = 0.10$, $x/D = 2$), and Run 49 ($W^* = 0.75$, $x/D = 4$). Corrisin (4) has measured values of turbulence in free jet mixing; from this report, fairly typical values of $\overline{u}'/U_r = 0.50$ and

$\overline{v}'/U_r = 0.25$ were assumed for the mixing regions. An examination of the velocity profiles reveals a definite mixing region $0.2 \leq (r/r_o)^2 \leq 0.7$ for Run 51 (Fig. 26), $0.1 \leq (r/r_o)^2$ for Run 64, and $0 \leq (r/r_o)^2 \leq 0.7$ for Run 49. The velocity correction, $U_{actual} \simeq 0.9\ U_{indicated}$ (see Appendix C for derivation), was applied to the profiles in these regions. The values of flow rate and K_m were found to be corrected by the following:

Run	x/D	$w_{m,corr.}/w_{m,uncorr.}$	$K_{m,corr.}/K_{m,uncorr.}$	% increase in K_m
51	2	0.945	1.034	3.4%
64	2	0.918	1.028	2.8%
49	4	0.998	1.003	0.3%

As the uncertainty in determining the K_m's is $\pm$ 2%, the total uncertainty in K_m due to both instrument uncertainty and turbulent velocity fluctuation is taken to be:

$x/D \geq 4$	$\pm$ 2%
$x/D \leq 4$	+1 to +5%

FIGURE 26

MOMENTUM AND FLOW RATE PROFILES

Illustrates effect of turbulence on the mixing tube flow rate and on K_m .

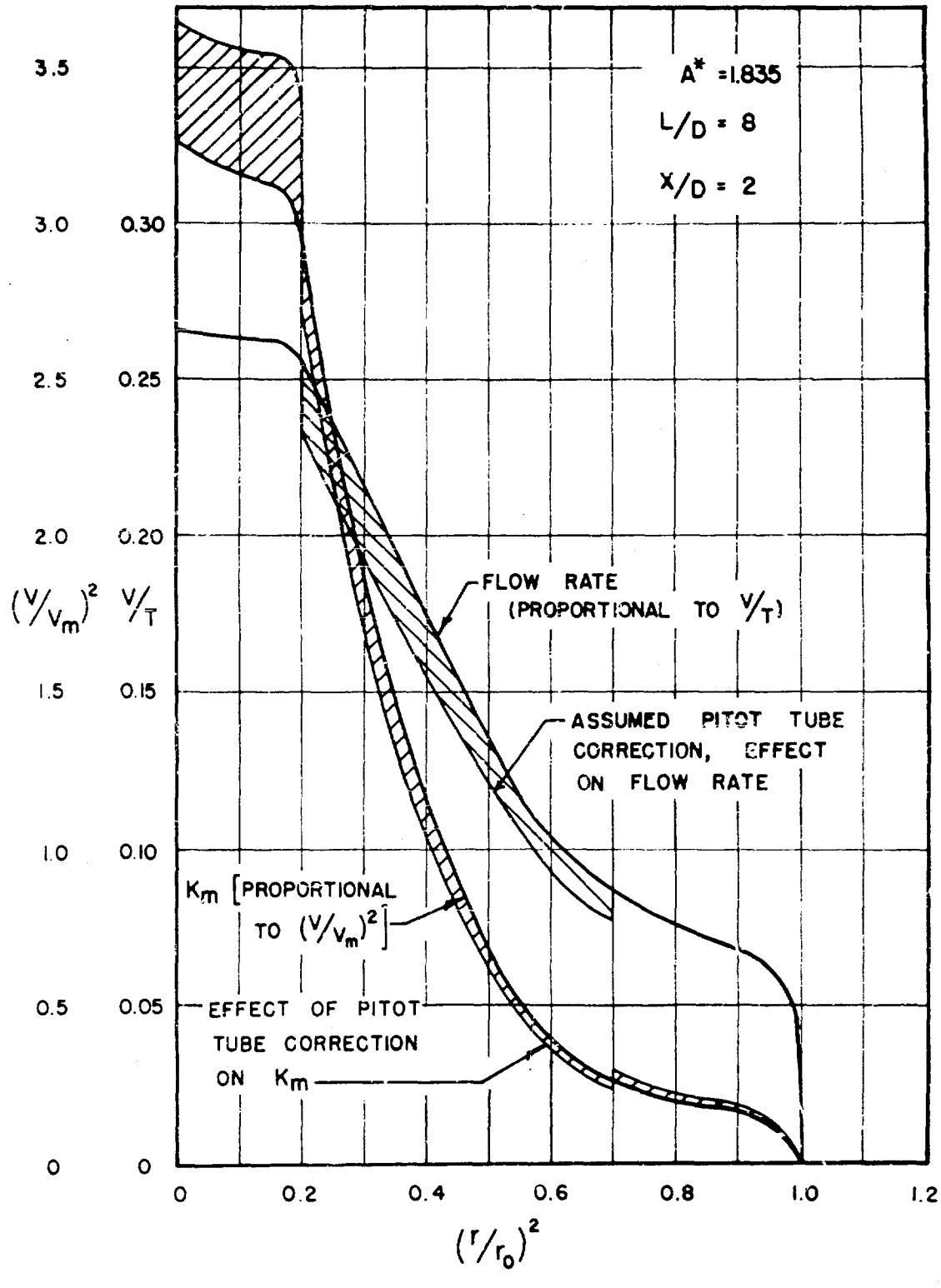
A* =1.835
L/D = 8
X/D = 2
FLOW RATE (PROPORTIONAL TO V/T)
ASSUMED PITOT TUBE CORRECTION, EFFECT ON FLOW RATE
Km [PROPORTIONAL TO (V/Vm)²]
EFFECT OF PITOT TUBE CORRECTION ON Km
(V/Vm)²
V/T
(r/r0)²
3.5
3.0
2.5
2.0
1.5
1.0
0.5
0
0.30
0.25
0.20
0.15
0.10
0.05
0
0.2
0.4
0.6
0.8
1.0
1.2

FIG. 26

APPENDIX C
ANALYSIS OF PITOT TUBE RESULTS

One of the primary objectives of this work was to establish confidence in the pitot tube traverse results by a comparison of the metered flow rate and that obtained by a velocity traverse. It was observed that the traverse results were consistently high, especially at low x/D's - from 2% at a W* of 1.0 to 10% at a W* of 0.1. This suggested a re-examination of Pitot tube results.

Goldstein (6) establishes that the equation of motion in the longitudinal direction for turbulent flow is

$$\frac{P}{\rho} + \frac{1}{2} U^2 + \frac{1}{2} \overline{q}'^2 = \frac{P_t}{\rho}$$

where P is the free stream pressure; U, the flow mean velocity; and $\overline{q}'$, the resultant turbulent velocity fluctuation,

$$\overline{q}' = \overline{u}'^2 + \overline{v}'^2 + \overline{w}'^2$$

The equation of motion in the transverse direction is

$$\frac{P}{\rho} + \frac{1}{2} \overline{v}'^2 = \frac{P_s}{\rho}$$

where $\overline{v}'$ is the transverse velocity fluctuation. The pitot static tube equation then becomes

$$\frac{(P_t - P_s)}{\rho} = \frac{1}{2} U^2 + \frac{1}{2} (\overline{q}'^2 - \overline{v}'^2)$$

or U, the mean velocity, must be calculated from

$$U = \sqrt{2 \left[\frac{(P_t - P_s)}{\rho} - \frac{1}{2} (\overline{q}'^2 - \overline{v}'^2) \right]}$$

In most turbulent flows, the turbulent components are negligible. However Corrisin (4) has studied the turbulent

fluctuations in free-jet mixing and found values of the ratio of the turbulent velocity fluctuation to local velocity in the neighborhood of $\overline{u}'/U_r = 0.50$ and $\overline{v}'/U_r = 0.25$ for the highly turbulent regions. These values of the fluctuating components would result in a pitot-static reading

$$\frac{(P_t - P_s)}{\rho} = 1.19\ U^2/2$$

The error in velocity, if the turbulent fluctuation is neglected in the calculation, is 9%. The effect on the traverse results by neglecting the turbulent fluctuations has also been observed by Nielsen (7) in comparing the flow metered by an orifice to that obtained by the integration of the velocity profile, the traverse being made a small distance behind the orifice. Here flow rate discrepancies from 5 to 16% were observed.

For highly turbulent regions of flow, some knowledge about the turbulent fluctuations is required if the velocities and flow rates are to be determined from Pitot traverses. If the data are not corrected for this effect, the calculated velocity will be higher than the actual, and the flow rate, proportional to the velocity, will likewise be high. This effect also indicates more complete mixing than actually occurs, with the result that the calculated K_m's are lower than the actual. These conclusions are supported in Appendix B, where a velocity profile was adjusted for this effect.

Another possibility for discrepancy exists if there is an appreciable transverse velocity component. In the mixing tube, this could be flow that spirals down the tube. A discrepancy is caused in that the pitot tube measures the total velocity head, even if misaligned as much as 20° with respect to the mean flow. The resultant velocity, of greater magnitude than the longitudinal or mean velocity, will be interpreted as the longitudinal velocity. The calculated velocity will then be larger than the actual longitudinal velocity. The flow angle can be determined with a yaw detector. The

results indicated an angle of about 2.5°, or 0.1% on velocity. The effect was negligible in this investigation.

A third type of error is introduced into the pitot tube results in that the flow is highly rotational. This causes a shifting, or curving, of the streamlines in the vicinity of the pitot tube nose such that the pitot tube "sees" a velocity higher than the velocity that would be there in the absence of the pitot tube. An empirical relation for the amount of shift is given by

$$\delta/D_{t0} = 0.131 + 0.082\ D_{t0}/D_{ti}$$

for

$$0.1 \leq \frac{D_{t0}}{U} \cdot \frac{dU}{dr} \leq 1.2 \quad , \quad (8)$$

where D_{t0} is the pitot tube outer diameter, 0.058"; D_{ti}, the inner diameter, 0.029" ; (dU/dr), the velocity gradient; and δ, the shift toward the low velocity region, $\delta \simeq 0.01"$, $\delta/r_o \simeq 0.007$. As the flow at $x/D \leq 2$ was of this type, this correction was effected on the raw data."